Mechanical expansion microscopy

Yuhang Fan[a,†], Youngbin Lim[a,†], Livia S. Wyss[b], Seongjin Park[c], Cancan Xu[e], Huikang Fu[e], Jingyi Fei[c,d], Yi Hong[e], Bo Wang[a,f,*]

[a]*Department of Bioengineering, Stanford University, Stanford, CA, United States*
[b]*Department of Biology, Stanford University, Stanford, CA, United States*
[c]*Department of Biochemistry and Molecular Biology, University of Chicago, Chicago, IL, United States*
[d]*Institute for Biophysical Dynamics, University of Chicago, Chicago, IL, United States*
[e]*Department of Bioengineering, University of Texas at Arlington, Arlington, TX, United States*
[f]*Department of Developmental Biology, Stanford University School of Medicine, Stanford, CA, United States*
**Corresponding author: e-mail address: wangbo@stanford.edu*

Chapter outline

[†]These authors contributed equally to this work.

Methods in Cell Biology, ISSN 0091-679X, https://doi.org/10.1016/bs.mcb.2020.04.013
© 2020 Elsevier Inc. All rights reserved.

ARTICLE IN PRESS

Abstract

This chapter describes two mechanical expansion microscopy methods with accompanying step-by-step protocols. The first method, mechanically resolved expansion microscopy, uses non-uniform expansion of partially digested samples to provide the imaging contrast that resolves local mechanical properties. Examining bacterial cell wall with this method, we are able to distinguish bacterial species in mixed populations based on their distinct cell wall rigidity and detect cell wall damage caused by various physiological and chemical perturbations. The second method is mechanically locked expansion microscopy, in which we use a mechanically stable gel network to prevent the original polyacrylate network from shrinking in ionic buffers. This method allows us to use anti-photobleaching buffers in expansion microscopy, enabling detection of novel ultra-structures under the optical diffraction limit through super-resolution single molecule localization microscopy on bacterial cells and whole-mount immunofluorescence imaging in thick animal tissues. We also discuss potential applications and assess future directions.

1 Introduction

1.1 Mechanically resolved expansion microscopy

Among super-resolution optical imaging techniques, expansion microscopy (ExM) is the only method that does not require expensive optics and special fluorophores (Chen, Tillberg, & Boyden, 2015; Chozinski et al., 2016; Tillberg et al., 2016; Wassie, Zhao, & Boyden, 2019). Instead, it relies on simple chemistry in which samples are anchored to a crosslinked polyelectrolyte hydrogel network and then expanded by the electrostatic repulsion between polymer chains. Cellular and tissue structures expand uniformly with the hydrogel as membranes and proteins are completely removed to diminish the mechanical strength of a cell. The "expanded" images are converted back to the original size for improved resolution.

In contrast to uniform expansion in typical ExM methods, we recently proposed the concept of mechanically resolved expansion microscopy (Lim et al., 2019), in which partially digested samples still retain partial mechanical strength and thereby are expanded nonuniformly. The nonuniformity in expansion provides information about the local mechanical properties of molecular and cellular components. Our first application of this concept used bacterial cells, taking advantage of the fact that their cell wall, a layer of peptidoglycan, is resistant to detergent and protease treatments in standard ExM protocols. As the bacterial cell wall is responsible for shape determination in virtually all bacteria and its mechanical properties vary widely across species and physiological conditions (Gan, Chen, & Jensen, 2008; Matias & Beveridge, 2005; Misra, Rojas, Gopinathan, & Huang, 2013; Tuson et al., 2012; Yao, Jericho, Pink, & Beveridge, 1999), we were able to use the contrast in cell wall expandability to resolve bacterial cells of different species or in distinct physiological states.

Fig. 1 summarizes our findings using mechanically resolved ExM to image bacteria that either express fluorescent proteins or are labeled by DNA stain. Digestion

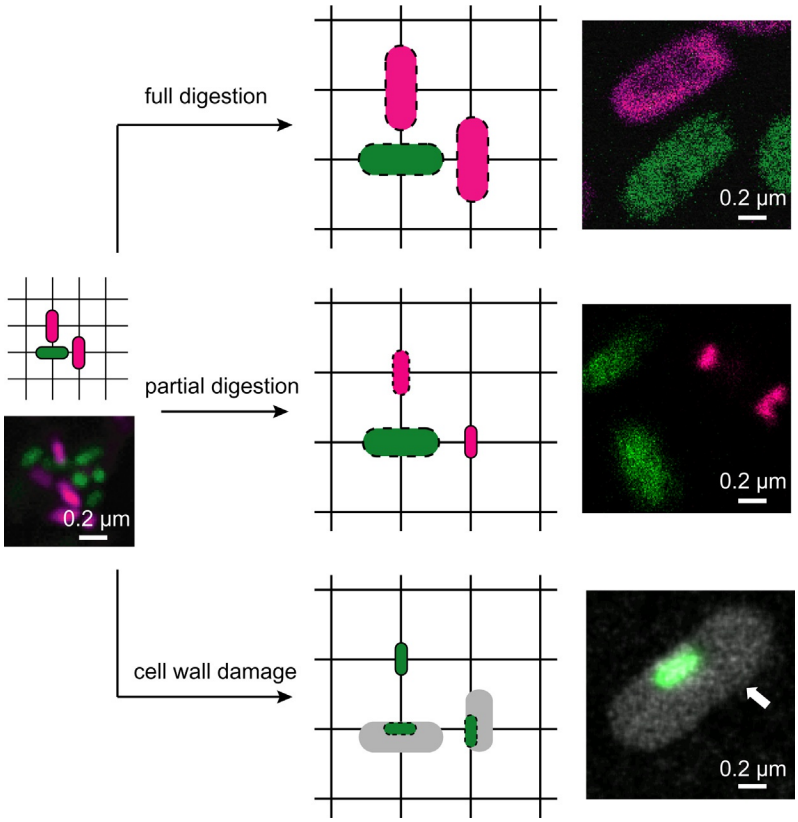

FIG. 1

Mechanically resolved ExM to image bacteria. Schematics and corresponding example microscopy images summarizing three experimental outcomes. Expansion of cells after full cell wall digestion using mutanolysin leads to uniform expansion of all cells (top). Expansion of cells after partial cell wall digestion using lysozyme enhances the contrast in expandability between cells of different cell wall rigidity (middle). Expansion of cells with cell wall damage leads to a large halo of DNA fluorescence surrounding the unexpanded cytoplasm (bottom). Microscopy images: left, a mixture of mCherry-*Lactobacillus plantarum* (magenta) and GFP-*Acetobacter tropicalis* (green) cells before expansion; right top, expanded *L. plantarum* and *A. tropicalis* cells after mutanolysin treatment; right middle, expanded *L. plantarum* and *A. tropicalis* cells after lysozyme treatment; right bottom, DNA-expanded GFP-*Salmonella* (green) cells at 3 h after being engulfed by a macrophage RAW264.7 cell, with DNA labeled by DAPI (gray). DNA chains (arrow) translocate through the pore in the cell wall and spread into the space surrounding the unexpanded cytoplasm.

All images are adapted from Lim, Y., Shiver, A., Khariton, M., Lane, K., Ng, K., Bray, S., et al. (2019). Mechanically resolved imaging of bacteria using expansion microscopy. PLoS Biology, 17*(10), e3000268; experimental procedures are detailed in the original study.*

of cell wall using highly potent muramidase, such as mutanolysin from *Streptomyces globisporus*, leads to uniform expansion of all cells and improves imaging resolution as is typical in ExM methods (Fig. 1, top right). Partial digestion of cell wall using mild muramidase, such as lysozyme from chicken egg white, enhances the contrast in expandability between cells of different cell wall rigidity. Cells with thin and weak walls can be expanded with differing degrees whereas cells with thick and tough walls remain mostly unexpanded (Fig. 1, middle right). This phenomenon provides a new quantitative imaging contrast that is informed by cell wall mechanics and orthogonal to spectral separation commonly used in optical microscopy. Finally, expansion is sensitive to local cell wall damage. Under this condition, the overall structure of the cell wall is still present and restricts the hydrogel network within (to which cytoplasmic proteins are anchored) from expanding whereas the extracellular network can expand freely. This non-uniform expansion creates a low-density cavity surrounding the cell and induces DNA to translocate through pores in the cell wall and occupy the extracellular cavity (Fig. 1, bottom right). We have used this phenomenon to quantify the kinetics of cell wall damage under antibiotic treatment as well as host cell defense mechanisms (Lim et al., 2019). Detailed protocols to implement these experiments are provided in Section 2.

Expansion phenotypes depend on the rupture point of the cell envelope, which may not necessarily correlate with the cell wall stiffness measured by conventional mechanical methods (e.g., atomic force microscopy (Gan et al., 2008; Rojas et al., 2018)). The rupture point is a more biologically relevant mechanical characteristic compared to stiffness, as it reflects the degree of stress that cells can tolerate before losing integrity. The stress can result from genetic disruption of cell wall synthesis or chemical perturbations such as antibiotic treatment (Coates et al., 2018; Huang, Mukhopadhyay, Wen, Gitai, & Wingreen, 2008), pH changes, and osmotic shock (Tropini et al., 2018). ExM can measure cell mechanics in vivo or in situ within a dense complex microbial population, and therefore, is expected to promote research on understanding how physical and biological environments modulate cell phenotypes.

Another important feature of mechanically resolved ExM is that it offers a sensitive measure to distinguish cells of different species in a mixed population based on the contrast in degree of expansion between cells. We expect this approach to be particularly useful in cases when fluorescent labeling and spectral imaging are restricted. For example, we used ExM to image populations of human commensal bacteria and measured, based on the distinct expansion patterns of cells, the abundance of individual species, which was then validated through complementary measurements of colony-forming units (Lim et al., 2019). Transforming these bacteria with fluorescent proteins has been challenging due to their current genetic intractability, and therefore species-specific fluorescent labeling has not been possible. This application demonstrates the unique utility of mechanically resolved ExM to understand the assembly and growth of mixed bacterial populations.

As another application, we imaged a model gut microbial community in the planarian flatworm, *Schmidtea mediterranea* (Fig. 2). The planarian is one of the most

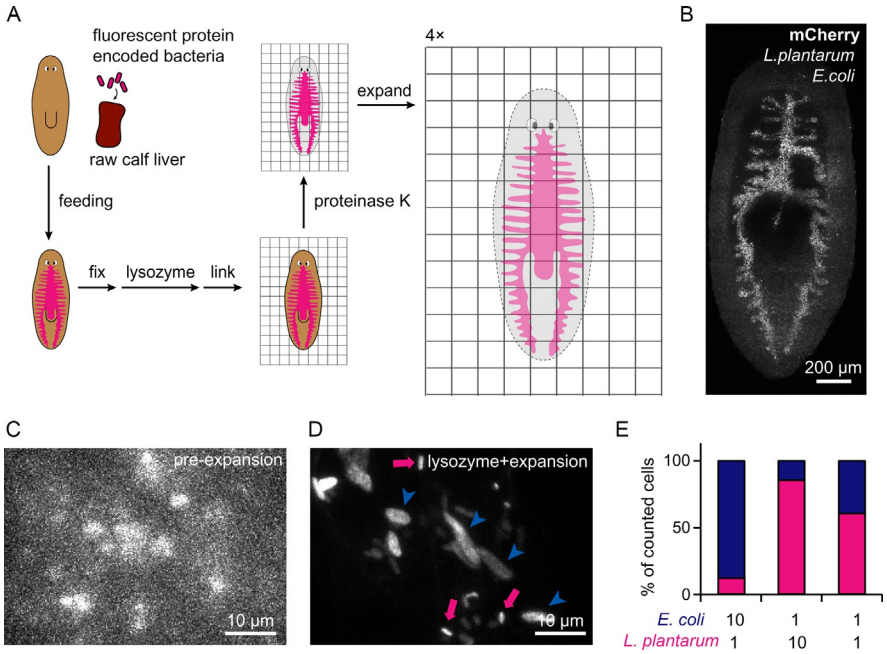

FIG. 2

Mechanically resolved ExM distinguishes different bacterial species in a model gut microbiota. (A) Schematic of the mechanically resolved ExM workflow for the planarian flatworm. Planarians were fed with mCherry-*L. plantarum* and mCherry-*E. coli* cells mixed in calf liver. After allowing the bacteria colonization to stabilize for 3 d, the planarians are fixed, and bacterial cell wall is digested by lysozyme in order to distinguish *L. plantarum* and *E. coli*. (B) Pre-expansion maximum-intensity projection image of a planarian with its gut colonized by *E. coli* and *L. plantarum*. (C and D) Magnified views showing microbial populations before expansion (C), and after expansion with lysozyme treatment (D). In (D), arrows: *L. plantarum* cells that are unexpanded; arrowheads: *E. coli* cells that are expanded by ~twofold. (E) Species composition in the planarian gut at 3 d post-feeding, quantified based on cell width determined on expansion images with lysozyme treatment. The relative abundance of the two species in the initial mixture fed to the planarians is specified below the plot.

All figures are adapted from Lim, Y., Shiver, A., Khariton, M., Lane, K., Ng, K., Bray, S., et al. (2019). Mechanically resolved imaging of bacteria using expansion microscopy. PLoS Biology, 17*(10), e3000268; experimental procedures are detailed in the original study.*

regenerative animals, able to regrow an entire body from a small tissue piece (Newmark & Alvarado, 2002; Reddien, 2018; Rink, 2013). Recently, the planarian's microbiota has been linked to its regenerative ability (Arnold et al., 2016; Lee, Williams, Levin, & Wolfe, 2018). In the planarian gut, the strong autofluorescence from the host tissue limits the usage of fluorescent labels that overlap with

autofluorescence spectrum. For this experiment, we colonized the planarian gut with *Escherichia coli* and *Lactobacillus plantarum*, both expressing mCherry and possessing similar size and morphology. While the two bacterial species were indistinguishable through fluorescence, they split into two populations after lysozyme treatment and expansion: *E. coli* cells expanded by approximately twofold and *L. plantarum* cells remained unexpanded (Fig. 2B). This clear separation allowed us to quantify the relative abundance of the two species of bacteria in the gut of the planarian, which corresponded to the initial mixture fed (Fig. 2C–E). These results demonstrate that ExM can be used to quantify species composition in vivo, a critical step toward determining the key factors that regulate the compositional dynamics of gut microbiota (Obadia et al., 2017; Vega & Gore, 2017).

1.2 Mechanically locked expansion microscopy

Section 3 details a method using ExM to image nanometer-scale ultra-structures in bacterial cells that are under the diffraction limit of optical imaging. This is possible only when the bacterial cell wall is predigested by mutanolysin to achieve uniform expansion. Recent progress has integrated ExM with other super-resolution imaging techniques, including stimulated emission depletion microscopy (STED) (Gao et al., 2018), structured illumination microscopy (SIM) (Halpern, Alas, Chozinski, Paredez, & Vaughan, 2017), and stochastic optical reconstruction microscopy (STORM) (Shi et al., 2019; Xu et al., 2019), for further improved "ultra" resolution. Our protocols focus on STORM imaging on expanded cells.

A common challenge in integrating super-resolution techniques with ExM is that these techniques typically use imaging buffers to control fluorophore photophysical kinetics and avoid photobleaching. However, the polyelectrolyte hydrogel network used in ExM (i.e., polyacrylamide-polyacrylate) shrinks dramatically in ionic buffers as electrostatic repulsion between polymer chains is screened by free ions. While previous studies have provided application-specific solutions, here we seek for a more widely applicable strategy.

We explore the concept of interpenetrating polymer networks (IPNs) where two polymers, often with different attributes, are interlaced within the same space to create new properties. We reasoned that IPNs formed by polyacrylamide-polyacrylate (PA) and another non-ionic hydrophilic polymer may provide mechanical support to counteract the deswelling tendency of the PA network alone, and thereby "lock" the size of the expanded samples (Fig. 3A). This second polymer must have compatible solubility with and match the mesh structure of PA networks so that microscopic phase separation does not occur. This is important because any network heterogeneity can scatter light and result in loss of optical transparency. We tested a series of hydrophilic polymers and found that poly(ethylene glycol) (PEG), with chain lengths between crosslinking points in the range of Mw ~3000–6000 Da, can form stable IPNs with PA (Table 1). PEG network interacts with water molecules through hydrogen bonds, therefore, its swelling property is independent of electrostatics and insensitive to surrounding ions (Fig. 3B).

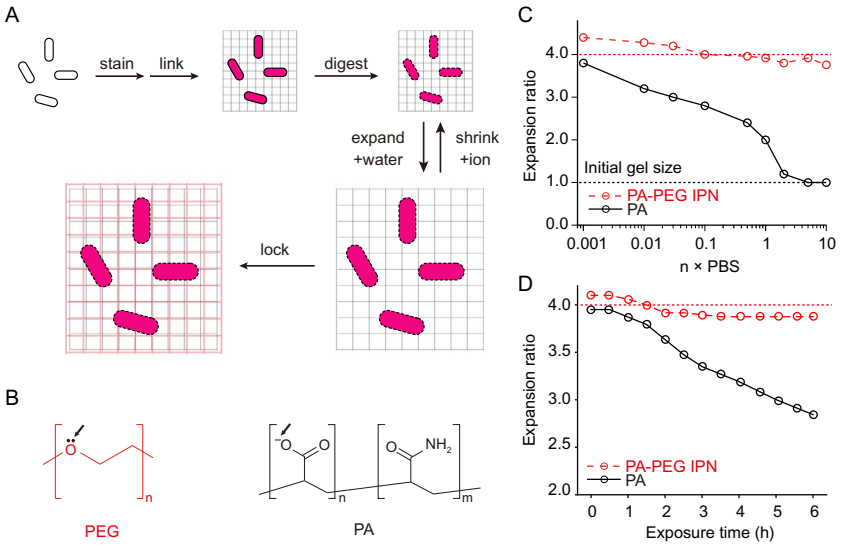

FIG. 3

Mechanically locked expansion microscopy solves the problem of buffer-induced sample shrinkage in ExM. (A) The workflow of locked-ExM. After expansion, a second non-ionic hydrogel network is formed to provide mechanical support for locking the size of the expanded sample. (B) Molecular structures of polyacrylamide-polyacrylate (PA) and poly(ethylene glycol) (PEG). PEG has no ionic group and forms hydrogen bonds with water through a lone pair (arrow, left), whereas PA carries a net negative charge (arrow, right). (C) Locked gels maintain their sizes in ionic buffer whereas un-locked gels shrink dramatically with increasing ionic strength. Gels are allowed to stabilize in buffer for ~1 h before measuring their sizes. (D) Locked gels maintain their sizes when exposed to ambient air whereas un-locked gels dry with time and shrink in size.

In our protocol, which is referred as "mechanically locked expansion microscopy" (locked-ExM), we form the PEG network within the expanded PA network using a photoinitiator (I-2959) to crosslink PEG diacrylate. PA-PEG IPNs have excellent optical transparency, and most importantly, the size of the expanded tissues is locked even in buffers with extreme ionic strengths, e.g., 10 × PBS (Fig. 3C). This property allows us to use a variety of anti-photobleaching buffers, including the standard STORM imaging buffer (i.e., 10 mM NaCl, 50 mM Tris, 10% glucose, pH = 8.0, with oxygen scavenger as 12 unit/mL of glucose oxidase and 900 unit/mL of catalase). By contrast, at the same salt concentration, PA networks shrink to the original, unexpanded size. An additional benefit of PEG locking is that the size of hydrogel remains rather stable even after being dried in ambient air for hours. This is important as one of the common technical difficulties in implementing ExM is that its PA hydrogel dries and shrinks quickly when exposed to air, often leading to significant lateral drift during long imaging periods (Fig. 3D).

Table 1 Test conditions to form PEG network in locked-ExM.

PEG molecular weight and concentration		
Molecular weight (Da)	**Concentration (%)**	**Result**
$M_n = 250$	1	Not soluble
	5	Not soluble
	10	Not soluble
$M_n = 575$	5	Gel expands by ~two fold, but deforms upon expansion
	10	Poor transparency
$M_n = 3400$	1	No gelation
	5	No gelation
	10	Gel with stable size
$M_n = 6000$	1	No gelation
	5	No gelation
	10	Gel with stable size
Initiator (test on PEG-DA, $M_n = 6000$)		
Initiator	**Concentration (%)**	**Result**
APS/TEMED	0.5	~30% size reduction during crosslinking
Lithium phenyl-2,4,6-trimethylbenzoylphosphinate (LAP)	0.5	>80% size reduction during crosslinking
I2959	0.05	No gelation
I2959	0.5	Gel with stable size

To optimize for expansion performance, we evaluated the influence of PEG molecular weight between crosslinks and the composition of crosslinking initiator. The final conditions are gray shaded.

Enabled by locked-ExM, we used STORM to image RNase E proteins in expanded bacterial cells (Fig. 4). RNase E is an essential enzyme for mRNA turnover in many bacteria (Mackie, 2013). Inhomogeneous intracellular distribution of RNase E can create spatial bias in regulating mRNA turnover at transcriptomic level (Moffitt, Pandey, Boettiger, Wang, & Zhuang, 2016), therefore, imaging the protein with high spatial resolution has been of major interest. In this experiment, we used an *E. coli* strain with endogenous *rne* gene fused with a Flag tag at the C-terminus. RNase E-Flag proteins were then labeled with immunofluorescence. We observed that RNase E proteins are localized to the cell periphery, forming foci with an average size of ~200 nm in expanded cells corresponding to 50 nm in diameter before expansion, a size well below the optical diffraction limit. This observation is consistent with the previous report that RNase E is associated with the cell membrane through a

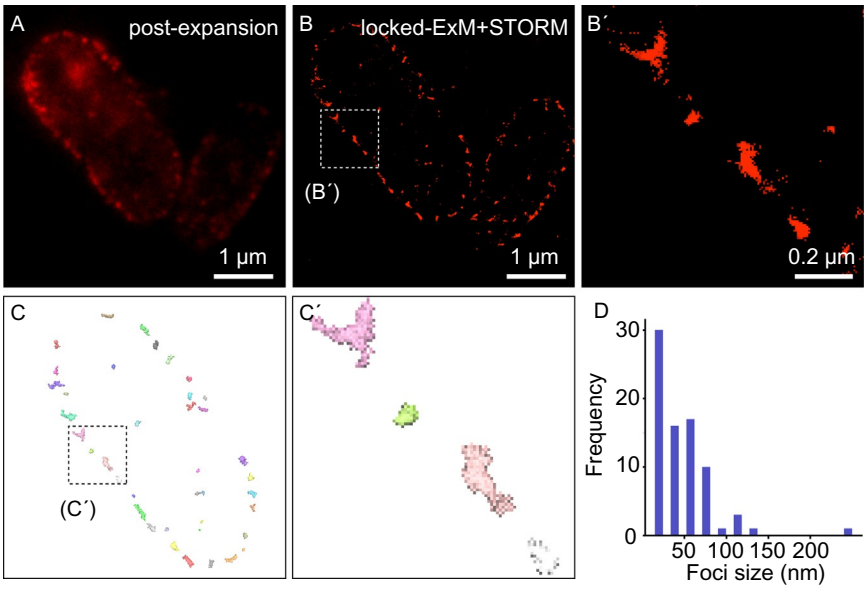

FIG. 4

Locked-ExM is integrated with STORM to image ultra-structures in bacterial cells. (A) Epifluorescence image (100×, oil immersion, NA = 1.49) of expanded *E. coli* cells with RNase E-Flag proteins labeled through immunofluorescence. (B) Corresponding reconstructed STORM image, with the boxed area shown in a magnified view (B′). RNase E protein foci localized to the cell periphery. (C) Cluster analysis quantifies foci size from the STORM image. Identified clusters are colored distinctly. A magnified view corresponding to the boxed area is shown in (C′). (D) Foci size distribution quantified from ~5 cells showing that the RNase E foci size is below the optical diffraction limit. Post-expansion dimensions have been converted to match the pre-expansion size.

specific membrane anchoring domain and can form dynamic foci on the membrane (Strahl et al., 2015). These results demonstrate that we are able to image structures in bacterial cells at the 10 nm scale by combining locked-ExM and STORM.

The last part of this chapter generalizes the methodology of locked-ExM for improving immunofluorescence in whole-mount thick animal tissues, such as the planarian. Applications of ExM in thick samples have been challenging, because long imaging times often lead to extensive photobleaching. In addition, expansion leads to a ~100-fold volumetric dilution of fluorophores and necessitates strong excitation to collect enough photons per volume, which in turn may accelerate photobleaching. Using PA-PEG IPNs, we are now able to apply anti-photobleaching systems (e.g., a cocktail of a triplet state quencher, trolox, and enzymatic oxygen scavengers) in ExM, which provides brighter and more stable fluorescence compared to imaging in pure water.

We used locked-ExM to resolve small anatomical structures in the planarian nervous system (Fig. 5), which are unresolvable under the conventional confocal microscopy. Other common super-resolution techniques (e.g., STORM or STED) are

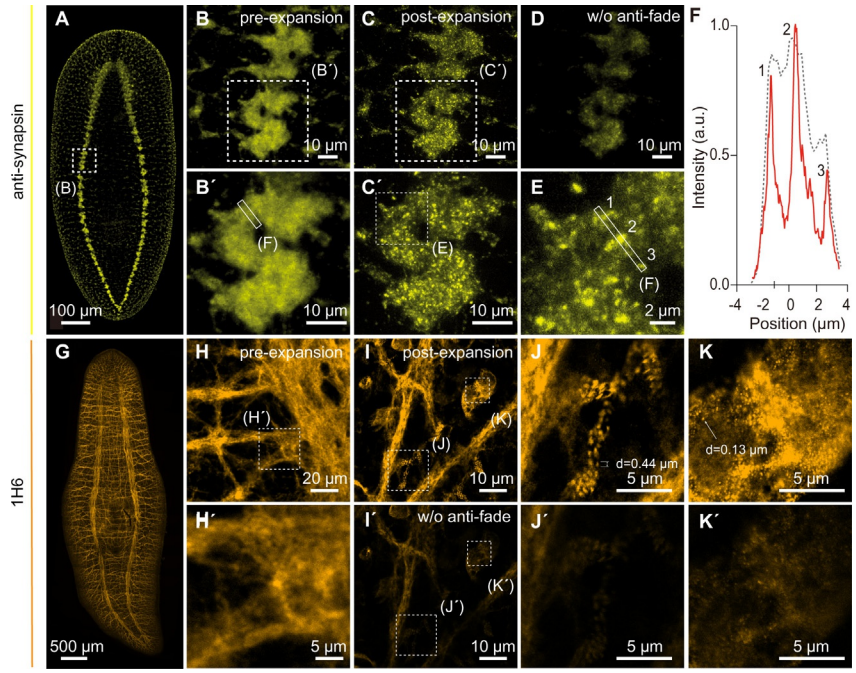

FIG. 5

Locked-ExM allows using anti-fade reagents and captures novel nanostructures in whole-mount imaging of the planarian nervous system. (A) Whole-mount view of a planarian immunostained by anti-synapsin. The boxed area in the nerve cord is serially magnified in (B) and (B′) with corresponding post-expansion images shown in (C) and (C′), respectively. The images are taken in anti-fade buffer. Note the contrast between the diffusive signal in pre-expansion images and punctate signal in post-expansion images, which are not visible when imaging without anti-fade buffer due to extensive photobleaching (D). We attribute the punctate signals to synaptic vesicles to which synapsins are known to bind. (E) Magnified view of the boxed region in (C′). (F) Cross-sectional normalized fluorescence intensity profiles of the regions highlighted in (B′, dotted gray line) and (E, red line) to show that locked-ExM resolves individual synaptic vesicles. (G) Whole-mount view of a planarian immunostained by 1H6, which labels neuronal cell bodies and processes in the planarian (Ross et al., 2015). (H) Magnified view of neuronal processes labeled by 1H6 before expansion with the boxed region magnified in (H′). (I) Locked-ExM resolves punctuate structures in the neural network, which are unresolvable in pre-expansion images. Boxed regions are magnified to show the nanostructures on neural processes (J) and neuronal cell body (K), respectively. Since the epitope of 1H6 is unknown, the molecular components of these structures remain to be identified. The post-expansion images are taken in anti-fade buffer. (I′–K′) Images corresponding to the same set of views in (I–K) taken without anti-fade, in which none of the punctuate structures are visible due to photobleaching. The sizes of representative nanostructures are specified in (J) and (K). Scale bars in the post-expansion image have been rescaled to match the pre-expansion dimensions.

not suitable either, as these neural structures are too deep in the tissues (~100 μm) for these techniques to reach. Even using ExM without anti-photobleaching, the signals of these structures were too weak to capture and quickly photobleached. In the first set of images, we captured synaptic vesicle-like structures in the planarian using confocal microscopy (Fig. 5A–F): the cross-sectional intensity profile of individual vesicles yielded an average vesicle size of 81 ± 8 nm (mean ± s.d., converted to the pre-expansion dimension), ~¼ of the diffraction limit. This size is consistent with previous transmission electron microscopy data (Brubacher, Vieira, & Newmark, 2014). In the second set of images, we captured a variety of nanostructures, distributed both on neuronal cell bodies and their long processes (Fig. 5G–K), which have not been resolved previously.

Although our locked-ExM protocols are implemented with immunofluorescence, it is also expected to be particularly useful for combining fluorescence in situ hybridization (FISH) and ExM for nanoscale imaging RNA molecules. As FISH protocols require ionic buffers for hybridization, the previous implementation of ExFISH (Chen et al., 2016; Moffitt, Hao, et al., 2016; Wang, Moffitt, & Zhuang, 2018) had to carefully balance the opposite needs of hybridization and expansion to reach a compromise. Now locked-ExM should provide a convenient solution.

2 Mechanically resolved expansion microscopy of bacteria

2.1 Rationale

In this section, we provide a generic protocol for using ExM to image bacterial cells, with complete or partial digestion of the cell wall depending on the application. As most ExM methods have focused on animal cells and tissues, our protocols also offer technical tips for implementing ExM on bacterial cells. We only list the equipment and reagents that are critical to reproduce our protocols; other common equipment and supplies, such as tubes, pipettes, dishes, shakers, slides, centrifuges, and pH meters, are omitted for brevity.

2.2 Materials, equipment, reagents

Biological materials

Bacterial cells are cultured in strain-specific media and conditions. We recommend using cells during the early stationary phase because the cell wall mechanical property changes during cell elongation (Misra et al., 2013). Indeed, we have noticed large cell-to-cell variations in expansion between dividing cells during exponential growth. We typically grow bacteria in 5 mL cultures overnight (~16 h) before ExM experiments.

Equipment and supplies

- Confocal microscope

  We use a Zeiss LSM 800 in an upright configuration equipped with a 20× water-immersion objective (W Plan-Apochromat, NA = 1.0, working

distance = 1.8 mm) and a 40× water-immersion objective (LD C-Apochromat Corr M27, NA = 1.1, working distance = 0.62 mm) mounted on an Axio Examiner. The upright configuration and the long working distance objectives are chosen for imaging thick samples after expansion.

- Incubator

  We use a hybridization oven (Fisher Scientific, cat. no. 13-247-10).
- Tweezers with soft tip (JETEHO, cat. no. B07P9GGF2K)

  The gel is fragile, in particular after expansion; we use soft-tip tweezers for gel handling to avoid damage.
- iSpacer (3.0-mm deep, Sunjin lab, cat. no. IS013)

Reagents

- 20× PBS (TEKNOVA, cat. no. P0191)
- Tris base (Fisher Scientific, cat. no. BP152-1)
- Acetic acid (Fisher Scientific, cat. no. A38-212)
- 0.5 M ethylenediaminetetraacetic acid (EDTA; Invitrogen, cat. no. 15575)
- Ammonium persulfate (APS; Thermo Scientific, cat. no. 17874)
- Sodium acrylate (Sigma-Aldrich, cat. no. 408220)
- 40% acrylamide (Bio-Rad, cat. no. 161-0140)
- 2% *N*,*N*′-methylenebisacrylamide (Bio-Rad, cat. no. 161-0142)
- 16% (w/v) formaldehyde (FA; Thermo Scientific, cat. no. 28906)

  FA is toxic upon inhalation, ingestion or contact with skin. Use protective gloves and handle with care in a ventilated hood.
- Nonidet P 40 substitute (NP-40; Sigma-Aldrich, cat. no. 74385)
- Triton X-100 (Fisher Scientific, cat. no. BP151)
- Potassium phosphate (Sigma-Aldrich, cat. no. P5629)
- 4-hyroxy-TEMPO (Sigma-Aldrich, cat. no. 176141)
- Tetramethylethylenediamine (TEMED; Thermo Scientific, cat. no. 17919)
- Guanidine hydrochloride (Thermo Scientific, cat. no. 24110)
- Methacrylic acid *N*-hydroxysuccinimide ester (MA-NHS; Sigma-Aldrich, cat. no. 730300)
- Dimethyl sulfoxide (DMSO; Sigma-Aldrich, cat. no. D5758)
- Mutanolysin (Sigma-Aldrich, cat. no. M9901)
- Lysozyme (Thermo Scientific, cat. no. 90082)
- Proteinase K (ProK; NEB, cat. no. P8107)
- TO-PRO-3 iodide solution (Invitrogen, cat. no. T3605)

Reagent setup

- PBSTx: 0.3% (w/v) Triton X-100 in PBS.
- TAE buffer: 40 mM Tris, 20 mM acetic acid, and 1 mM EDTA in MilliQ H_2O.
- Fixative: 4% (w/v) FA and 1% (w/v) NP-40 in PBS. This solution should be made fresh in a fume hood. As NP-40 is highly viscous, we recommend making 10% stock solution in PBS to be diluted to a final concentration of 1%.
- MA-NHS stock solution: 1 M MA-NHS in DMSO. This solution can be stored at −20 °C for several months and diluted in PBS at 1:1000 before use.

ARTICLE IN PRESS

- Phosphate buffer: 50 mM potassium phosphate in MilliQ H_2O. Adjust pH to 4.9. This solution should be made fresh before use.
- Monomer solution: 2 M NaCl, 2.5% (w/w) acrylamide, 0.15% (w/w) bisacrylamide, 8.625% (w/w) sodium acrylate in PBS. This solution can be stored at −20 °C for up to 1 month. We have noticed large batch-to-batch inconsistency in sodium acrylate quality even when reagents are purchased from the same manufacturer. This batch effect can affect expansion significantly. For every new bottle, we recommend making a 33% (w/v) sodium acrylate stock to ensure that the solution is colorless under ambient light.
- Gelation solution: 0.01% (v/v) 4-hydroxy-TEMPO, 0.2% (w/v) APS, and 0.2% (v/v) TEMED in monomer solution. This solution should be made fresh on ice just before the gelation step. APS is diluted from a 10% stock solution made in water, which can be stored at 4 °C for up to 1 week, and should be added last.
- Digestion buffer: 0.5% Triton X-100, 0.8 M guanidine HCl, and 8 units/mL Proteinase K in TAE. This solution can be stored as aliquots at −20 °C for up to one month, with ProK added just before use.

2.3 Protocols

Sample preparation

1. Collect cells from 5 mL of overnight cultures via centrifugation at 2000 g for 5 min. Resuspend the pellet in 1 mL of PBS and transfer to a 1.7 mL tube. Wash twice via repeated centrifugation and resuspension.
2. Fix cells in 1 mL of fixative with agitation for 10 min.
3. Pellet cells and remove the fixative. Wash cells in PBS and then resuspend in 1 mL of PBSTx by gentle pipetting. Incubate cells for 30 min at room temperature on a nutator to permeabilize the membrane.
4. Replace PBSTx with 1 mL of 50% methanol in PBSTx and agitate for 10 min.
5. Replace 50% methanol with 1 mL of 100% methanol. Dehydrated cells are kept in methanol at −20 °C for at least 2 h. In these dehydration steps, ethanol can be used in place of methanol, with the final step in 70% ethanol.
6. Rehydrate cells by incubating in 1 mL of 50% methanol in PBSTx at room temperature for 10 min, and then in PBSTx for 10 min. The dehydration steps are optional but provide two benefits. First, they further fix the cells by inducing protein precipitation and remove lipids to enhance permeability. Second, dehydrated samples are highly stable and can be stored for at least several months at −20 °C. However, we also note that, in immunofluorescence experiments, some epitopes can be destroyed upon dehydration. Under those situations, dehydration should be omitted.

Expansion

7. Remove PBSTx and digest cell walls by incubating in either 1 mL of PBS containing 1 mg/mL lysozyme or phosphate buffer containing 160 unit/mL mutanolysin in a 1.7 mL tube on a rotor overnight at 37 °C. Afterwards, wash in PBS three times for 5 min each. This step is omitted in experiments that aim for detecting cell wall damage.

ARTICLE IN PRESS

8. Incubate in 1 mL of 1 mM MA-NHS in PBS for 1 h at room temperature to attach chemical anchors to proteins. Wash in PBS three times.
9. Replace PBS with 100 μL of monomer solution and incubate for 1 min. The incubation time should be extended to 45 min at 4 °C if the samples are bacteria cells contained in host cells or tissues.
10. Prepare gelation chambers following the procedure depicted in Fig. 6.
11. Slowly pipette cell suspension into the gelation chamber from one of the open edges of the gelation chamber.
12. Pipette ~200 μL of gelation solution to fill the chamber and then allow the gelation to proceed for 2 h at 37 °C. During this step, cells should mostly sediment to the glass slide surface.
13. Remove the top coverslip from the chamber, cut the gel into ~5 mm squares using a razor blade, and transfer the gel in a 24-well plate using soft-tip tweezers. The gel can be imaged in PBS at this step to determine unexpanded cell size.
14. Add 1.5 mL of digestion buffer into the well, seal with parafilm to prevent evaporation, and incubate overnight at 37 °C.
15. Transfer the gel in a 60-mm petri dish using tweezers and fill the dish with MilliQ H_2O. Gradually increasing the amount of water helps prevent the gel from folding. Allow the gel to expand for 45 min, change water every 15 min. At the final water change, 1 μM TO-PRO-3 can be added to stain DNA.

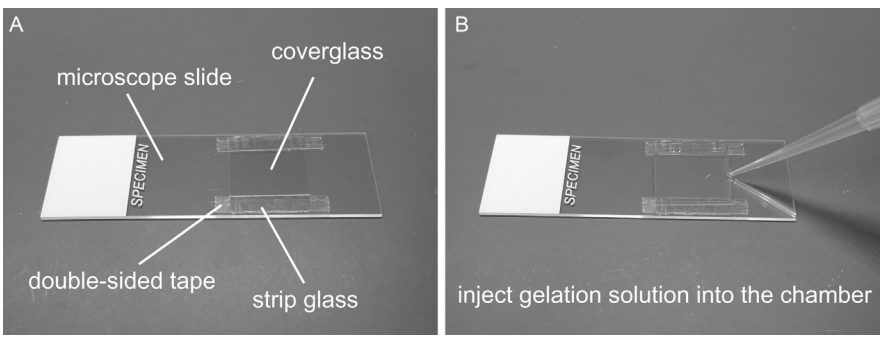

FIG. 6

Assembly of gelation chamber. (A) To assemble the gelation chamber, two glass stripes (~3 × 20 mm) are cut from #1 coverglass using a diamond cutter and taped on a coverslip using double-sided tape. On top of the stripes, another #1.5 coverglass is placed gently. For thick tissues, we use 2–3 stacked glass strips as the spacer. (B) Monomer and gelation solutions are pipetted on one side of the chamber and drawn into the chamber by capillary force.

ARTICLE IN PRESS

Imaging and analyses

16. Cut the expanded gel into 2–4 cm edge-length rectangles to fit on a coverglass and gently place another coverglass on top for imaging. The gel is oriented as such that the side with cells faces toward the objective. To avoid lateral drift during long image acquisition, mount expanded gels in imaging chambers assembled from iSpacer sandwiched between two coverslips and filled with MilliQ water. Immobilize the gel using a small amount of cyanoacrylate or epoxy glue on the periphery to fully prevent image drift.
17. Image with 1 Airy Unit pinhole, and average for 16 scans to reduce noise.
18. Large views are captured as tiled images, which are stitched together using either Zen (Zeiss) or FIJI software. Maximum intensity projection images were generated using built-in functions. The FIJI plugin "MorphoLibJ" is used for segmenting bacterial cells. Cell width is measured along the short axis and averaged at five locations evenly spaced along the long axis manually or through a custom MATLAB script. The expansion ratio is computed as the average cell width in post-expansion images divided by the average cell width in pre-expansion images. The mean and variance of expansion ratio are determined from >5 confocal images, each containing hundreds of cells, collected from at least two independent experiments.

3 Mechanically locked expansion microscopy for super-resolution imaging

3.1 Rationale

This section provides protocols to implement locked-ExM, in which a second network of PEG is formed within the network of PA to lock the gel in its expanded size. This method releases the constraint in buffer usage of ExM and enables using anti-photobleaching buffers during imaging.

Our protocols include two applications. In the first application, we perform STORM imaging on expanded bacterial cells. STORM imaging requires using a complex buffer (10 mM NaCl, 50 mM Tris, with oxygen scavengers) with a high ionic strength that is not compatible with the original PA gel. In the second application, we examine the nervous system in whole-mount planarians, which are challenging to image as the signal is weak, scattered by the thick tissues, and due to long imaging times often photobleached. As shown below, adding anti-photobleaching buffer has enabled us to resolve structures that are invisible otherwise. We have included the labeling procedures for these applications in our protocols as well. To enhance fluorescence signal, we use tyramide signal amplification (TSA) instead of fluorophore conjugated secondary antibodies (King & Newmark, 2013). In the TSA reaction, peroxidase attached to secondary antibody catalyzes the covalent deposition of tyramide on and near a target protein in situ, generating high density labeling for improved sensitivity.

3.2 Materials, equipment, reagents

Biological materials

- *E. coli* strain with endogenous *rne* gene fused with a Flag tag at the C-terminus

  Cells are collected and fixed following the "Sample preparation" protocol described in Section 2.3. RNase E proteins are stained through anti-Flag primary antibody recognized by peroxidase conjugated secondary antibody followed by TSA reaction, and imaged using STORM.
- The planarian *Schmidtea mediterranea*

  We use the asexual strain (CIW4) for whole-mount immunofluorescence imaging. Planarians are maintained in 0.5 g/L Instant Ocean Sea Salts supplemented with 0.1 g/L sodium bicarbonate and fed calf liver paste once or twice weekly. Planarians are starved at least 5 d prior to all experiments. Before immunostaining, planarians are removed from salts, killed in 2% HCl on ice for 5 min, fixed in 4% FA in PBSTx for 15 min at room temperature.

Equipment and supplies

- STORM setup

  STORM is performed on a custom built setup previously described (Park, Zhang, et al., 2018). Briefly, an inverted optical microscope (Nikon Ti-E with a TIRF oil immersion objective, 100× NA = 1.49 CFI HP) is fiber-coupled with a 647 nm laser (Cobolt 06-01) for imaging and a 405 nm laser (Crystalaser) for fluorophore reactivation. A dichroic mirror (Chroma zt405/488/561/647/752r-UF3) is used for both lasers, and an emission filter (Chroma ET700/75M) is used for collecting Atto 655 fluorescence. The emission signal was captured by an EMCCD camera (Andor iXon Ultra 888). The *Z*-drift is prevented in real time by a built-in focus lock system (Nikon Perfect Focus).
- Poly-L-lysine coated glass slides (Sigma-Aldrich, cat. no. P0425)
- UV illuminator

  We use a UV bench lamp (UVP, cat. no. 95-0042-07) at a power density of 4 mW/cm^2. Avoid direct eye and skin exposure under UV.

Reagents

- PEG (MW = 6000, Sigma-Aldrich, cat. no. 81260)
- Dichloromethane (DCM; Sigma-Aldrich, cat. no. DX0835)
- Triethylamine (Sigma-Aldrich, cat. no. 471283 or T0886)
- Acryloyl chloride (Sigma-Aldrich, cat. no. A24109)
- Diethyl ether (Avantor, cat. no. 9244-05)
- Irgacure 2959 (Sigma-Aldrich, cat. no. 410896)
- Atto 655 NHS ester (Sigma-Aldrich, cat. no. 076245)
- TAMRA succinimidyl ester (Invitrogen, cat. no. C1171)
- Tyramine hydrochloride (Sigma-Aldrich, cat. no. T2879)
- 4-Iodophenylboronic acid (4-IPBA; Sigma-Aldrich, cat. no. 471933)
- Dimethylformamide (DMF; Sigma-Aldrich, cat. no. 227056 or D4551)
- Glucose (Sigma-Aldrich, cat. no. G7021)

- Boric acid (Fisher Scientific, cat. no. A73-500)
- Hydrogen peroxide (H_2O_2; Sigma-Aldrich, cat. no. H1009)
- Proteinase K (ProK; Thermo Fisher Scientific, cat. no. 25-530-049).
  This ProK is used to permeabilize planarian tissues in the immunofluorescence protocol, and different from the one used for the digestion of tissues in the ExM protocol.
- Sodium dodecyl sulfate (SDS; Fisher Scientific, cat. no. BP166-100)
- Catalase (Sigma-Aldrich, cat. no. G1345)
- Glucose oxidase (Sigma-Aldrich, cat. no. G2133)
- Trolox (Sigma-Aldrich, cat. no. 238813)
- β-D-glucose (TCI, cat. no. G0047)
- Mouse anti-FLAG (Sigma-Aldrich, cat. no. F1804)
- Mouse anti-SYNORF1 (DSHB, cat. no. 3C11)
- Mouse 1H6-E9 (DSHB, cat. no. 1H6-E9)
- Peroxidase conjugated goat anti-Mouse IgG + IgM (Jackson ImmunoResearch, cat. no. 115-035-044)
- Bovine serum albumin (BSA; Jackson ImmunoResearch, cat. no. 001-000-162)

Reagent setup

- PEG diacrylate (PEG-DA): while PEG-DA is available through multiple sources (e.g., Sigma-Aldrich), we have noticed large batch-to-batch quality inconsistency in these commercial products. Therefore, we have chosen to synthesize PEG-DA in house based on a method previously described (Xu, Lee, Dai, & Hong, 2018). Briefly, 20 g of PEG (MW = 6000) is dissolved in 15 mL of DCM. Under N_2 purge, 1.35 g of triethylamine in 15 mL of DCM is added to the PEG solution dropwise at room temperature. After 30 min, 1.078 mL of acryloyl chloride in 15 mL of DCM is added dropwise. The reaction is allowed to proceed for another 30 min. The mixture is then heated to 40 °C for 24 h. After returning to room temperature, the product is precipitated in ice-cold diethyl ether and filtered. The PEG-DA is dried in a vacuum chamber at room temperature for 2 d, and re-dissolved in MilliQ H_2O followed by another 2 d of dialysis (MWCO 2kD, SpectrumLab). The solution is lyophilized to obtain the final product.
- PEG-DA solution: 10% (w/w) PEG-DA and 0.5% (w/w) irgacure 2959 in MilliQ H_2O. This solution needs to be made fresh before use.
- TEG buffer: 25 mM Tris-HCl, 10 mM EDTA, 50 mM glucose in MilliQ H_2O, pH adjusted to 8. This solution needs to be made fresh before use.
- ProK solution: 2 μg/mL ProK and 0.1% SDS in PBSTx. This solution need to be made fresh before use with ProK added last.
- Tyramide: following previously published procedure (King & Newmark, 2013), tyramide conjugated fluorophores are synthesized by mixing stock solutions of tyramine hydrochloride (10 mg/mL in DMF) containing triethylamine (10 μg/mL), and NHS ester (10 mg/mL in DMF) for 2 h at room temperature. Fresh anhydrous DMF should be used for this reaction. The mixing ratio should

ARTICLE IN PRESS

give ~1.1-fold molar excess of NHS ester to tyramine, and needs to be protected from light throughout the reaction. The product is diluted to 1 mg/mL with ethanol and can be stored at −20 °C for at least a year.
- TSA buffer: 2 M NaCl and 0.1 M boric acid in MilliQ H_2O, pH adjusted to 8.5. Filter to sterilize. This solution can be stored at 4 °C for several months.
- 4-IPBA solution: 20 mg/mL 4-IPBA in DMF. This solution can be stored at −20 °C for several months.
- TSA solution: tyramide conjugated fluorophores (1:500 dilution from stock solution), 4-IPBA (1:1000 dilution from stock solution), and 0.003% H_2O_2 in TSA buffer. This solution needs to be made fresh before use with H_2O_2 added last.
- STORM imaging buffer: 10 mM NaCl, 50 mM Tris, 10% β-D-glucose, with oxygen scavenger (12 unit/mL glucose oxidase and 900 unit/mL catalase) in MilliQ H_2O. Imaging buffer without the oxygen scavenger can be kept at room temperate. The oxygen scavenger needs to be added to the buffer freshly before use.
- Anti-fade buffer: 7.5 unit/mL glucose oxidase, 1000 unit/mL catalase, 50 mM β-D-glucose, and 2 mM trolox in 100 mM Tris-HCl (pH = 8). This solution needs to be made fresh before use.

3.3 Protocols

Immunostaining of bacteria

1. Pipette 100 µL of rehydrated cells in PBS, prepared as previously described in Section 2.3, on a poly-L-lysine coated microscope glass slide and incubate for 1.5 h at 4 °C. Wash to remove unattached cells.
2. Pipette ~500 µL of 25 µg/mL lysozyme in TEG buffer onto the slide. Incubate for 30 min at room temperature. Wash twice with PBS. TEG buffer contains EDTA that permeabilizes the outer membrane by removing Mg^{2+} and Ca^{2+}.
3. Remove PBS and incubate the cells in 2% BSA in PBS for 1 h at room temperature.
4. Exchange BSA with mouse anti-FLAG (1:400 dilution in PBS) and incubate for 1 h. Wash three times in PBS with 5 min each.
5. Incubate in peroxidase conjugated goat anti-Mouse (1:200 dilution in PBS) for 1 h. Wash three times in PBS.
6. Incubate in TSA solution for 10 min. This step needs to be protected from light. Wash three times.

Immunostaining for planarian

1. Bleach freshly fixed planarians overnight in 6% H_2O_2 in PBSTx under direct light. Wash in PBSTx three times for 5 min each. We typically treat ~3 animals in a 1.7 mL tube.
2. Permeabilize tissues by incubating in 1 mL of ProK solution for 10 min at room temperature.
3. Post-fix in 1 mL of 4% FA in PBSTx for 10 min. Wash in PBSTx three times.

ARTICLE IN PRESS

4. Exchange PBSTx with 1 mL of 1% BSA in PBSTx and incubate for 4 h at room temperature.
5. Incubate samples in 1 mL of anti-SYNORF1 or 1H6 (1:1000 in 1% BSA) overnight at 4 °C. Wash in PBSTx six times with each for 1 h.
6. Incubate in 1 mL of 1% BSA in PBSTx for 4 h at room temperature.
7. Remove BSA and add 1 mL of peroxidase conjugated goat anti-Mouse (1:1000 in 1% BSA) overnight at 4 °C. Wash in PBSTx six times with each for 1 h.
8. Remove PBSTx, add 1 mL of TSA solution, and incubate for 10 min protected from light. Wash three times. DAPI can be added during the washing steps to stain DNA.

Locked-ExM

1. Follow the "Expansion" protocol in Section 2.3, except the cell wall digestion step. For planarian, we extend the incubation time in monomer solution to 45 min at 4 °C.
2. Incubate the expanded gel (2–4 cm in size) in 2 mL of PEG-DA solution overnight at room temperature. This step needs to be protected from light.
3. Remove the gel from PEG-DA solution and wick away excess solution from the edges. This step is critical as it allows forming the PEG network only within but not outside the PA network. We note that having PEG network outside causes compression of the PA gel and a ~30% sample size reduction.
4. Immediately irradiate the gel with UV light (4 mW/cm^2) for 10 min.
5. Mount the gel for imaging following the steps described in the "Imaging and analyses" protocol in Section 2.3. For STORM imaging, the power density of the 647 nm laser is ~2300 W/cm^2, and the power density of the 405 nm laser was modulated gradually up to ~16 W/cm^2 for capturing reasonable number of spots per frame. Samples are soaked in the STORM imaging buffer throughout the imaging. The images are reconstructed digitally as previously described (Fei et al., 2015; Rust, Bates, & Zhuang, 2006). For confocal microscopy, samples are imaged in anti-fade buffer.
6. To quantify the size of RNase E clusters in STORM images, clusters are identified using the density-based spatial clustering of applications with noise (DBSCAN) method (Daszykowski, Walczak, & Massart, 2002; Park, Bujnowska, McLean, & Fei, 2018). We empirically determine the two parameters, the minimum distance between two points in a cluster and the minimum number of points to define a cluster. From the resulting clusters, the cluster center is defined as the vector average of points comprising the cluster. We measure their size as the twice of the average distance from the cluster center to every point in the cluster.

4 Discussion and conclusions

In this chapter, we provide the detailed protocols of two mechanical expansion microscopy methods: mechanically resolved ExM and mechanically locked-ExM.

In contrast to most ExM methods that rely on uniform sample expansion to improve imaging resolution, mechanically resolved ExM builds on the concept that non-uniform expansion of partially digested cells and tissues provides information about local mechanical properties in the sample. While we have used this information to inspect bacterial cell walls, similar strategies are expected to be widely applicable to image other groups of organisms, including algae, fungi, and plants, which also have cell walls. Because cell walls can have species-specific biochemical compositions, extending mechanically resolved imaging to non-bacterial organisms requires testing other cell wall digestive enzymes. More broadly, it remains to be seen whether the same concept can be used to examine the mechanical properties and aggregation states of proteins and nucleic acids by using selective proteolytic enzymes or restriction endonucleases to partially digest these biomolecular components in order to induce contrast in their expandability.

The second technique, locked-ExM, addresses the common problem in ExM that polyacrylamide-polyacrylate (PA) gels shrink in ionic buffer, which is required by most anti-photobleaching systems and various staining techniques such as fluorescence in situ hybridization for imaging nucleic acids. Our solution is to introduce a secondary polymer network, poly(ethylene glycol) (PEG), to lock the size of expanded PA gels, as PEG lacks ionic groups and interacts with water molecules through hydrogen bonding independent of the electrostatics between PA chains and salt ions. Enabled by locked-ExM, we have implemented two applications that are both photon demanding and susceptible to photobleaching: STORM imaging of bacterial cells and super-resolution immunofluorescence imaging in whole-mount thick animal tissues. Looking forward, locked-ExM may represent only one of the first examples that exploit materials science concepts and tools in the vast chemical space of hydrogels to improve expansion microscopy techniques and develop new imaging methods to study biology.

Acknowledgments

We thank B. Pearson, R. Zayas, and J. Brubacher for discussions, E. Massé for sharing the Flag-tagged RNase E *E. coli* strain. L.S.W. is supported by a NIH Cellular, Biochemical, and Molecular Sciences (CMB) training grant (T32GM007276), and an NSF GFRP fellowship. S.P. acknowledges the support of the Yen postdoctoral fellowship from The University of Chicago. J.F. acknowledges the support from the Searle Scholars Program, NIH Director's New Innovator Award (1DP2GM128185-01), and NIH (R01 GM092830-06A1). Y.H. acknowledges the support from a NSF CAREER award (#1554835). This work is funded by a NSF-EDGE grant (IOS-1923534) to B.W.

References

Arnold, C. P., Shane Merryman, M., Harris-Arnold, A., McKinney, S. A., Seidel, C. W., Loethen, S., et al. (2016). Pathogenic shifts in endogenous microbiota impede tissue regeneration via distinct activation of TAK1/MKK/p38. *eLife, 5*, e16793.

Brubacher, J. L., Vieira, A. P., & Newmark, P. A. (2014). Preparation of the planarian *Schmidtea mediterranea* for high-resolution histology and transmission electron microscopy. *Nature Protocols*, *9*(3), 661–673.

ARTICLE IN PRESS

Chen, F., Tillberg, P. W., & Boyden, E. S. (2015). Expansion microscopy. *Science*, *347*(6221), 543–548.

Chen, F., Wassie, A. T., Cote, A. J., Sinha, A., Alon, S., Asano, S., et al. (2016). Nanoscale imaging of RNA with expansion microscopy. *Nature Methods*, *13*(8), 679–684.

Chozinski, T. J., Halpern, A. R., Okawa, H., Kim, H. J., Tremel, G. J., Wong, R. O. L., et al. (2016). Expansion microscopy with conventional antibodies and fluorescent proteins. *Nature Methods*, *13*(6), 485–488.

Coates, J., Park, B. R., Le, D., Şimşek, E., Chaudhry, W., & Kim, M. (2018). Antibiotic-induced population fluctuations and stochastic clearance of bacteria. *eLife, 7*, e32976.

Daszykowski, M., Walczak, B., & Massart, D. L. (2002). On the optimal partitioning of data with K-means, growing K-means, neural gas, and growing neural gas. *Journal of Chemical Information and Computer Sciences*, *42*(6), 1378–1389.

Fei, J., Singh, D., Zhang, Q., Park, S., Balasubramanian, D., Golding, I., et al. (2015). Determination of in vivo target search kinetics of regulatory noncoding RNA. *Science*, *347*(6228), 1371–1374.

Gan, L., Chen, S., & Jensen, G. J. (2008). Molecular organization of Gram-negative peptidoglycan. *Proceedings of the National Academy of Sciences of the United States of America*, *105*(48), 18953–18957.

Gao, M., Maraspini, R., Beutel, O., Zehtabian, A., Eickholt, B., Honigmann, A., et al. (2018). Expansion stimulated emission depletion microscopy (ExSTED). *ACS Nano*, *12*(5), 4178–4185.

Halpern, A. R., Alas, G. C. M., Chozinski, T. J., Paredez, A. R., & Vaughan, J. C. (2017). Hybrid structured illumination expansion microscopy reveals microbial cytoskeleton organization. *ACS Nano*, *11*(12), 12677–12686.

Huang, K. C., Mukhopadhyay, R., Wen, B., Gitai, Z., & Wingreen, N. S. (2008). Cell shape and cell-wall organization in Gram-negative bacteria. *Proceedings of the National Academy of Sciences of the United States of America*, *105*(49), 19282–19287.

King, R. S., & Newmark, P. A. (2013). In situ hybridization protocol for enhanced detection of gene expression in the planarian *Schmidtea mediterranea*. *BMC Developmental Biology*, *13*(1), 8.

Lee, F. J., Williams, K. B., Levin, M., & Wolfe, B. E. (2018). The bacterial metabolite indole inhibits regeneration of the planarian flatworm Dugesia japonica. *iScience*, *10*, 135–148.

Lim, Y., Shiver, A., Khariton, M., Lane, K., Ng, K., Bray, S., et al. (2019). Mechanically resolved imaging of bacteria using expansion microscopy. *PLoS Biology, 17*(10), e3000268.

Mackie, G. A. (2013). RNase E: At the interface of bacterial RNA processing and decay. *Nature Reviews Microbiology*, *11*(1), 45–57.

Matias, V. R. F., & Beveridge, T. J. (2005). Cryo-electron microscopy reveals native polymeric cell wall structure in *Bacillus subtilis* 168 and the existence of a periplasmic space. *Molecular Microbiology*, *56*(1), 240–251.

Misra, G., Rojas, E. R., Gopinathan, A., & Huang, K. C. (2013). Mechanical consequences of cell-wall turnover in the elongation of a Gram-positive bacterium. *Biophysical Journal*, *104*(11), 2342–2352.

Moffitt, J. R., Hao, J., Bambah-Mukku, D., Lu, T., Dulac, C., & Zhuang, X. (2016). High-performance multiplexed fluorescence in situ hybridization in culture and tissue with matrix imprinting and clearing. *Proceedings of the National Academy of Sciences of the United States of America*, *113*(50), 14456–14461.

Moffitt, J. R., Pandey, S., Boettiger, A. N., Wang, S., & Zhuang, X. (2016). Spatial organization shapes the turnover of a bacterial transcriptome. *eLife*, *5*, 13065.

ARTICLE IN PRESS

Newmark, P. A., & Alvarado, A. S. (2002). Not your father's planarian: A classic model enters the era of functional genomics. *Nature Reviews Genetics*, *3*(3), 210–219.

Obadia, B., Güvener, Z. T., Zhang, V., Ceja-Navarro, J. A., Brodie, E. L., Ja, W. W., et al. (2017). Probabilistic invasion underlies natural gut microbiome stability. *Current Biology*, *27*(13), 1999–2006.

Park, S., Bujnowska, M., McLean, E. L., & Fei, J. (2018). Quantitative super-resolution imaging of small RNAs in bacterial cells. *Methods in Molecular Biology*, *1737*, 199–212.

Park, S., Zhang, J., Reyer, M. A., Zareba, J., Troy, A. A., & Fei, J. (2018). Conducting multiple imaging modes with one fluorescence microscope. *Journal of Visualized Experiments, 140*, e58320.

Reddien, P. W. (2018). The cellular and molecular basis for planarian regeneration. *Cell*, *175*(2), 327–345.

Rink, J. C. (2013). Stem cell systems and regeneration in planaria. *Development Genes and Evolution*, *223*(1–2), 67–84.

Rojas, E. R., Billings, G., Odermatt, P. D., Auer, G. K., Zhu, L., Miguel, A., et al. (2018). The outer membrane is an essential load-bearing element in Gram-negative bacteria. *Nature*, *559*(7715), 617.

Ross, K. G., Omuro, K. C., Taylor, M. R., Munday, R. K., Hubert, A., King, R. S., et al. (2015). Novel monoclonal antibodies to study tissue regeneration in planarians. *BMC Developmental Biology*, *15*(1), 2.

Rust, M. J., Bates, M., & Zhuang, X. (2006). Sub-diffraction-limit imaging by stochastic optical reconstruction microscopy (STORM). *Nature Methods*, *3*(10), 793.

Shi, X., Li, Q., Dai, Z., Tran, A., Feng, S., Ramirez, A. D., et al. (2019). Label-retention expansion microscopy. *bioRxiv*, 687954.

Strahl, H., Turlan, C., Khalid, S., Bond, P. J., Kebalo, J. M., Peyron, P., et al. (2015). Membrane recognition and dynamics of the RNA degradosome. *PLoS Genetics, 11*(2), e1004961.

Tillberg, P. W., Chen, F., Piatkevich, K. D., Zhao, Y., Yu, C. C., English, B. P., et al. (2016). Protein-retention expansion microscopy of cells and tissues labeled using standard fluorescent proteins and antibodies. *Nature Biotechnology*, *34*(9), 987.

Tropini, C., Moss, E. L., Merrill, B. D., Ng, K. M., Higginbottom, S. K., Casavant, E. P., et al. (2018). Transient osmotic perturbation causes long-term alteration to the gut microbiota. *Cell*, *173*(7), 1742–1754.

Tuson, H. H., Auer, G. K., Renner, L. D., Hasebe, M., Tropini, C., Salick, M., et al. (2012). Measuring the stiffness of bacterial cells from growth rates in hydrogels of tunable elasticity. *Molecular Microbiology*, *84*(5), 874–891.

Vega, N. M., & Gore, J. (2017). Stochastic assembly produces heterogeneous communities in the *Caenorhabditis elegans* intestine. *PLoS Biology, 15*(3), e2000633.

Wang, G., Moffitt, J. R., & Zhuang, X. (2018). Multiplexed imaging of high-density libraries of RNAs with MERFISH and expansion microscopy. *Scientific Reports*, *8*(1), 4847.

Wassie, A. T., Zhao, Y., & Boyden, E. S. (2019). Expansion microscopy: Principles and uses in biological research. *Nature Methods*, *16*(1), 33–41.

Xu, C., Lee, W., Dai, G., & Hong, Y. (2018). Highly elastic biodegradable single-network hydrogel for cell printing. *ACS Applied Materials and Interfaces*, *10*(12), 9969–9979.

Xu, H., Tong, Z., Ye, Q., Sun, T., Hong, Z., Zhang, L., et al. (2019). Molecular organization of mammalian meiotic chromosome axis revealed by expansion STORM microscopy. *Proceedings of the National Academy of Sciences of the United States of America*, *116*(37), 18423–18428.

Yao, X., Jericho, M., Pink, D., & Beveridge, T. (1999). Thickness and elasticity of Gram-negative murein sacculi measured by atomic force microscopy. *Journal of Bacteriology*, *181*(22), 6865–6875.